Single-bubble dynamics in liquid nitrogen

Kyuichi Yasui
Department of Physics, Waseda University, 3-4-1 Ohkubo, Shinjuku, Tokyo, Japan
(Received 2 February 1998)

Computer simulations of bubble oscillations induced by an ultrasonic wave in liquid nitrogen are performed, including the effect of evaporation and condensation of nitrogen vapor at the bubble wall, that of droplets formation inside the bubble, and that of thermal conduction both inside and outside the bubble. Baghdassarian, Cho, Varoquaux, and Williams [J. Low. Temp. Phys. **110**, 305 (1998)] monitored the oscillations of a helium bubble in liquid nitrogen by scattering an argon-ion laser beam from the bubble and observed anomalous behavior of the intensity of the scattered light as a function of time. The results of the computer simulations in the present study indicate that the anomalous behavior observed is due to the light scattering from fine droplets created inside the bubble. It is also clarified that the bubble collapse under a condition of stable oscillations in liquid nitrogen is much milder than that in water at room temperature due to the much larger saturated vapor pressure of liquid nitrogen. As the result, the maximum temperature attained in the bubble in liquid nitrogen is much lower than that required for single-bubble sonoluminescence. [S1063-651X(98)03907-5]

PACS number(s): 47.55.Bx, 78.60.Mq

I. INTRODUCTION

Observations of a single-bubble sonoluminescence (SBSL) were reported less than ten years ago [1–3]. SBSL is a light emission phenomenon from a stably oscillating bubble in liquid irradiated by ultrasonic wave. The light is emitted at the collapse of the bubble. The pulse width of the light is experimentally measured to range from 50 to 250 ps [2,4,5]. The spectrum is broadband and can be fitted by a blackbody formula with the effective temperatures ranging from 6000 K to 50 000 K [6–8]. The light pulse is emitted periodically with the frequency of the ultrasonic wave [4].

The mechanism of the light emission of SBSL is not yet understood, though several theories have been proposed, such as the shock-wave theory [9–12] in which a spherical shock wave converges at the center of the bubble and light is emitted by thermal bremsstrahlung from the plasma formed by the shock-wave convergence, and the hot-spot theory [13–15] where the bubble is heated by quasiadiabatic compression and thermal radiation is emitted. Since most of the SBSL intensity is in the ultraviolet in many experiments [6], Williams and his co-workers [16,17] have attempted to observe SBSL in liquid nitrogen whose absorption in the ultraviolet is much less than that of water. Single bubbles of helium gas of radius 10–20 μm have been stably trapped in liquid nitrogen for several minutes at the pressure antinode of the standing acoustic wave [16,17], though no SBSL has yet been observed [17]. The bubble oscillations are monitored by scattering a 100 mW argon-ion laser beam from the bubble and the anomalous behavior of the intensity of the scattered light is observed as a function of time [17].

In the present study, computer simulations of bubble oscillations in liquid nitrogen are performed in order to study the anomalous behavior observed [17], including the effect of evaporation and condensation of nitrogen vapor at the bubble wall, that of droplets formation inside the bubble, and that of thermal conduction both inside and outside the bubble.

II. MODEL

The physical situation is that of a single spherical bubble in liquid nitrogen irradiated by an ultrasonic wave. The bubble consists of helium and nitrogen vapor. Pressure (p_g) inside a bubble is assumed to be spatially uniform. The temperature inside a bubble is assumed to be spatially uniform except at the thermal boundary layer near the bubble wall. The width of the thermal boundary layer is assumed to be $n\lambda$, where n is a constant and λ is the mean free path of a gas molecule [18]. In the present calculations, $n=7$ is assumed [18]. It is assumed that the temperature in the boundary layer changes linearly with radius (r): from T at $r=R-n\lambda$ to T_B at $r=R$, where R is the bubble radius and T_B is the gas-temperature at the bubble wall [the origin of the radius (r) is the bubble center] [18]. Thus

$$\left.\frac{\partial T}{\partial r}\right|_{r=R}=\frac{T_B-T}{n\lambda}. \tag{1}$$

The mean free path (λ) is calculated by Eq. (2) [19].

$$\lambda=\frac{(V-V_d)}{\sqrt{2}\sigma' n_t}, \tag{2}$$

where V is the volume of the bubble, V_d is the total volume of droplets inside the bubble, σ' is the cross section of a molecule in the bubble [in this calculation, $\sigma'=0.4\times10^{-18}(\mathrm{m}^2)$ is employed], and n_t is the total number of molecules inside the bubble.

As a well known result of the kinetic theory of gases, temperature jump (ΔT) exists at the bubble wall [20].

$$T_B=T_{L,i}+\Delta T, \tag{3}$$

where $T_{L,i}$ is the liquid temperature at bubble wall. A temperature jump (ΔT) is given by Eq. (4) [20]:

$$\Delta T = -\frac{1}{2kn'}\left(\frac{\pi m}{2kT_B}\right)^{1/2}\frac{2-a'\alpha_e}{\alpha_e}\,\kappa\frac{\partial T}{\partial r}\bigg|_{r=R}, \tag{4}$$

where k is the Boltzmann constant, n' is the number density of gas molecules in the bubble, m is the mean mass of a molecule, α_e is the thermal accommodation coefficient, a' is a constant ($a'=0.827$ [20]), and κ is the thermal conductivity of the gas.

The thermal conductivity (κ) is calculated as a function of temperature by Eq. (5) [21]:

$$\kappa = (0.025+4.5\times10^{-4}T)\left(\frac{n_{\mathrm{He}}}{n_t}\right) + (0.0004+8.9\times10^{-5}T)\left(\frac{n_{\mathrm{N_2}}}{n_t}\right) \tag{5}$$

where κ is in W/m K and T is in K, and n_{He} ($n_{\mathrm{N_2}}$) is the number of helium (nitrogen) molecules in the bubble.

In the model, the number of nitrogen molecules in the bubble ($n_{\mathrm{N_2}}$) changes with time due to evaporation or condensation at the bubble wall and to formation or evaporation of fine droplets inside the bubble:

$$n_{\mathrm{N_2}}(t+\Delta t) = n_{\mathrm{N_2}}(t) + 4\pi R^2\dot{m}\,\frac{10^3N_A}{M_{\mathrm{N_2}}}\,\Delta t - \frac{4}{3}\,\pi r_*^3\rho_L\,\frac{10^3N_A}{M_{\mathrm{N_2}}}\,\Delta' N, \tag{6}$$

where t is the time, $\dot{m}$ is the net rate of evaporation at the bubble wall per unit area and unit time in kg/m^2 s (when $\dot{m}<0$, condensation takes place), N_A is the Avogadro number, $M_{\mathrm{N_2}}$ is the molar weight of nitrogen in g/mol, r_* is the radius of a droplet, ρ_L is the liquid density, and $\Delta' N$ is the change of the number of droplets in time Δt. The prime means that it excludes the contribution of the deposit of droplets onto the bubble wall. Details of the droplets formation and reduction are described later. The rate of evaporation at the bubble wall per unit area and unit time ($\dot{m}$) is calculated by Eqs. (7)–(9) [22–24]:

$$\dot{m} = \dot{m}_{\mathrm{eva}} - \dot{m}_{\mathrm{con}}, \tag{7}$$

$$\dot{m}_{\mathrm{eva}} = \frac{\alpha_M}{(2\pi R_v)^{1/2}}\,\frac{p_v^*}{T_{L,i}^{1/2}}, \tag{8}$$

$$\dot{m}_{\mathrm{con}} = \frac{\alpha_M}{(2\pi R_v)^{1/2}}\,\frac{\Gamma p_v}{T_B^{1/2}}. \tag{9}$$

Equation (7) means that the net rate of evaporation ($\dot{m}$) is the difference between the actual rate of evaporation ($\dot{m}_{\mathrm{eva}}$) and that of condensation ($\dot{m}_{\mathrm{con}}$). In Eqs. (8) and (9), α_M is the accommodation coefficient for evaporation or condensation, R_v is the gas constant of nitrogen vapor in (J/kg K), p_v^* is the saturated vapor pressure at temperature $T_{L,i}$, and p_v is the actual vapor pressure;

$$p_v = \frac{n_{\mathrm{N_2}}}{n_t}\,p_g. \tag{10}$$

The correction factor (Γ) in Eq. (9) is

$$\Gamma = \exp(-\Omega^2) - \Omega\sqrt{\pi}\left(1-\frac{2}{\sqrt{\pi}}\int_0^{\Omega}\exp(-x^2)dx\right), \tag{11}$$

where

$$\Omega = \frac{\dot{m}}{p_v}\left(\frac{R_vT}{2}\right)^{1/2}. \tag{12}$$

The accommodation coefficient (α_M) is assumed to be $\alpha_M=0.1$ in the present calculations. The saturated vapor pressure (p_v^*) is calculated as a function of temperature by the empirical formula given in the Appendix.

As the equation of bubble radius (R), Eq. (13) is employed, in which the compressibility of liquid and the effect of evaporation and condensation of nitrogen vapor at the bubble wall are taken into account [the derivation of Eq. (13) is given in Ref. [24]]:

$$\left(1-\frac{\dot{R}}{c}+\frac{\dot{m}}{c\rho_L}\right)R\ddot{R}+\frac{3}{2}\,\dot{R}^2\left(1-\frac{\dot{R}}{3c}+\frac{2\dot{m}}{3c\rho_L}\right) = \frac{1}{\rho_L}\left(1+\frac{\dot{R}}{c}\right)\left(p_B-p_s\left(t+\frac{R}{c}\right)-p_\infty\right)+\frac{\ddot{m}R}{\rho_L}\left(1-\frac{\dot{R}}{c}+\frac{\dot{m}}{c\rho_L}\right) + \frac{\dot{m}}{\rho_L}\left(\dot{R}+\frac{\dot{m}}{2\rho_L}+\frac{\dot{m}\dot{R}}{2c\rho_L}\right)+\frac{R}{c_\infty\rho_L}\,\frac{dp_B}{dt}, \tag{13}$$

where the dot denotes the time derivative (d/dt), c is the sound speed in the liquid, $p_B(t)$ is the liquid pressure on the external side of the bubble wall, $p_s(t)$ is a nonconstant ambient pressure component such as a sound field, and p_∞ is the undisturbed pressure. $p_B(t)$ is related to the pressure inside the bubble [$p_g(t)$] by Eq. (14) [23,24]:

$$p_B(t) = p_g(t) - \frac{2\sigma}{R} - \frac{4\mu}{R}\left(\dot{R}-\frac{\dot{m}}{\rho_L}\right) - \dot{m}^2\left(\frac{1}{\rho_L}-\frac{1}{\rho_g}\right), \tag{14}$$

where σ is the surface tension, μ is the liquid viscosity, and ρ_g is the density inside the bubble. When a bubble is irradi-

ated by an acoustic wave of which wavelength is much larger than the bubble radius, $p_s(t) = -A \sin \omega t$ where A is the pressure amplitude of the acoustic wave and ω is its angular frequency.

In order to calculate $p_g(t)$, the van der Waals equation of state is employed:

$$\left(p_g(t) + \frac{a}{v^2} \right)(v - b) = R_g T, \tag{15}$$

where a and b are the van der Waals constants, v is the molar volume, R_g is the gas constant, and T is the temperature inside the bubble. In this model, the van der Waals constants (a and b) change with time due to the change of the nitrogen content in the bubble by evaporation or condensation, according to Eqs. (16) and (17).

$$a = a_{\mathrm{He}} \left(\frac{n_{\mathrm{He}}}{n_t} \right)^2 + 2a_{\mathrm{He\text{-}N_2}} \left(\frac{n_{\mathrm{He}}}{n_t} \right) \left(\frac{n_{\mathrm{N_2}}}{n_t} \right) + a_{\mathrm{N_2}} \left(\frac{n_{\mathrm{N_2}}}{n_t} \right)^2, \tag{16}$$

$$b = b_{\mathrm{He}} \left(\frac{n_{\mathrm{He}}}{n_t} \right)^2 + 2b_{\mathrm{He\text{-}N_2}} \left(\frac{n_{\mathrm{He}}}{n_t} \right) \left(\frac{n_{\mathrm{N_2}}}{n_t} \right) + b_{\mathrm{N_2}} \left(\frac{n_{\mathrm{N_2}}}{n_t} \right)^2, \tag{17}$$

where a_{He} and b_{He} ($a_{\mathrm{N_2}}$ and $b_{\mathrm{N_2}}$) are the van der Waals constants of helium (nitrogen), $a_{\mathrm{He\text{-}N_2}} = \sqrt{a_{\mathrm{He}} a_{\mathrm{N_2}}}$, $\sqrt[3]{b_{\mathrm{He\text{-}N_2}}} = \frac{1}{2}(\sqrt[3]{b_{\mathrm{He}}} + \sqrt[3]{b_{\mathrm{N_2}}})$ [25]. The values are as follows [19]: $a_{\mathrm{He}} = 3.4 \times 10^{-3}$(J m^3/mol^2), $a_{\mathrm{N_2}} = 1.39 \times 10^{-1}$(J m^3/mol^2), $b_{\mathrm{He}} = 2.37 \times 10^{-5}$(m^3/mol), $b_{\mathrm{N_2}} = 3.913 \times 10^{-5}$(m^3/mol).

The temperature inside the bubble (T) is calculated by solving Eq. (18):

$$E = \frac{n_{\mathrm{He}}}{N_A} C_{V,\mathrm{He}} T + \frac{n_{\mathrm{N_2}}}{N_A} C_{V,\mathrm{N_2}} T - \left(\frac{n_t}{N_A} \right)^2 \frac{a}{V}, \tag{18}$$

where E is the thermal energy of the bubble, $C_{V,\mathrm{He}}$($C_{V,\mathrm{N_2}}$) is the molar heat of helium (nitrogen) at constant volume. The molar heat is assumed as follows; $C_{V,\mathrm{He}} = \frac{3}{2} R_g$ and $C_{V,\mathrm{N_2}} = \frac{5}{2} R_g$ [26]. The change of the thermal energy of a bubble (ΔE) in time Δt is expressed by [15]

$$\begin{aligned} \Delta E(t) = & - p_g(t) \Delta V(t) + 4\pi R^2 \dot{m} \frac{10^3 N_A}{M_{\mathrm{N_2}}} e_{\mathrm{N_2}} \Delta t \\ & + 4\pi R^2 \kappa \left. \frac{\partial T}{\partial r} \right|_{r=R} \Delta t + \frac{4}{3} \pi r_*^3 \rho_L L \Delta' N \\ & + \left[- \frac{3}{5} M \dot{R} \ddot{R} \right] \Delta t, \end{aligned} \tag{19}$$

where $e_{\mathrm{N_2}}$ is the energy carried by an evaporating or condensing vapor molecule, L is the latent heat of evaporation, and M is the total mass of the gases inside the bubble. The first term in the right hand side of Eq. (19) is the work by the surrounding liquid (pV work). The second term is the energy carried by evaporating or condensing vapor molecules. The third term is the energy change due to thermal conduction. The fourth term is the latent heat of droplets formation or evaporation. The last term is the change of the kinetic energy of gases into heat. The brackets mean that this term is included only when the term is positive, which corresponds to the decrease of the kinetic energy. When the term is negative, it is replaced by zero.

The energy carried by an evaporating or condensing vapor molecule $e_{\mathrm{N_2}}$ is calculated by Eq. (20) [27],

$$e_{\mathrm{N_2}} = \frac{C_{V,\mathrm{N_2}}}{N_A} T_B. \tag{20}$$

Following is the description on the variation of liquid temperature at the bubble wall [24]. Continuity of energy flux at the bubble wall is given by Eq. (21):

$$\kappa_L \left. \frac{\partial T_L}{\partial r} \right|_{r=R} = \kappa \left. \frac{\partial T}{\partial r} \right|_{r=R} + \dot{m} L + \frac{10^3 \dot{m}}{M_{\mathrm{N_2}}} C_{V,\mathrm{N_2}} (T_B - T_{L,i}), \tag{21}$$

where κ_L is the thermal conductivity of liquid nitrogen, and $T_L(r)$ is the liquid temperature at radius r. In this model, $\partial T_L / \partial r|_{r=R}$ is calculated by Eq. (21).

The spatial distribution of the liquid temperature [$T_L = T_L(r)$] should satisfy the following boundary conditions:

$$T_L(R) = T_{L,i}, \tag{22}$$

$$\left. \frac{\partial T_L(r)}{\partial r} \right|_{r=R} = \left. \frac{\partial T_L}{\partial r} \right|_{r=R}, \tag{23}$$

$$T_L(r \to \infty) = T_\infty, \tag{24}$$

$$\left. \frac{\partial T_L(r)}{\partial r} \right|_{r \to \infty} = 0, \tag{25}$$

where T_∞ is the ambient liquid temperature. In the present model, the temperature profile in the liquid is assumed to be exponential [Eqs. (26) and (27)].

When $(T_{L,i} - T_\infty) \partial T_L / \partial r|_{r=R} < 0$,

$$T_L(r) = (T_{L,i} - T_\infty) \exp\left(- \frac{\partial T_L / \partial r|_{r=R}}{(T_\infty - T_{L,i})} (r - R) \right) + T_\infty. \tag{26}$$

When $(T_{L,i} - T_\infty) \partial T_L / \partial r|_{r=R} > 0$

$$T_L(r) = A \exp[-B(r - C)^2] + T_\infty, \tag{27}$$

where

$$A = (T_{L,i} - T_\infty) \exp(B e_1^2),$$

$$B = \frac{\partial T_L / \partial r|_{r=R}}{2(T_{L,i} - T_\infty)} \frac{1}{e_1},$$

$$C = R + e_1,$$

$$e_1 = e_0 \left| \frac{T_{L,i} - T_B}{\partial T_L / \partial r|_{r=R}} \right|,$$

where e_0 is a parameter, which was determined to fit the calculated result of a radius-time curve with the experimental

data [28] of a bubble in water in the previous paper by the author [24]. The value is $e_0=1\times10^{-3}$ [24]. Both Eqs. (26) and (27) satisfy the boundary conditions [Eqs. (22)–(25)].

In the present model, a boundary layer is assumed in liquid phase near a bubble. The thickness of the layer (δ_L) is assumed as Eqs. (28) and (29).

When $(T_{L,i}-T_\infty)\partial T_L/\partial r|_{r=R}<0$,

$$\delta_L=\frac{T_\infty-T_{L,i}}{\partial T_L/\partial r|_{r=R}}. \tag{28}$$

When $(T_{L,i}-T_\infty)\partial T_L/\partial r|_{r=R}>0$

$$\delta_L=\frac{1}{\sqrt{B}}+e_1. \tag{29}$$

Variation of the liquid temperature at bubble wall ($T_{L,i}$) is calculated by Eq. (30),

$$T_{L,i}(t+\Delta t)=T_{L,i}(t)+\frac{4\pi R^2 j_1\Delta t-4\pi(R+\delta_L)^2 j_2\Delta t}{\frac{4}{3}\pi[(R+\delta_L)^3-R^3]\rho_L c_p}, \tag{30}$$

where $j_1(j_2)$ is the energy flux at $r=R(r=R+\delta_L)$ per unit area and unit time, and c_p is the specific heat of liquid nitrogen at constant pressure. j_1 and j_2 are calculated by Eqs. (31) and (32):

$$j_1=-\kappa_L|_{r=R}\left.\frac{\partial T_L}{\partial r}\right|_{r=R}, \tag{31}$$

$$j_2=-\kappa_L|_{r=R+\delta_L}\left.\frac{\partial T_L}{\partial r}\right|_{r=R+\delta_L}. \tag{32}$$

The assumed profile of liquid temperature [Eqs. (26) and (27)] is used only in the calculation of j_2 in Eq. (32).

Next the calculation method of droplet formation and reduction inside the bubble is described. The nucleation rate of fine droplets is given by the kinetic theory of liquids [29,30]:

$$J=\left(\frac{2\sigma_* m_{N_2}}{\pi}\right)^{1/2}\frac{1}{\rho_L}\left(\frac{p_v}{kT}\right)^2\exp\left(-\frac{4\pi r_c^2\sigma_*}{3kT}\right), \tag{33}$$

where σ_* is the effective surface tension of liquid nitrogen, m_{N_2} is the mass of a nitrogen molecule, and r_c is the critical droplet radius. Kawada and Mori [31] reported that the experimental nucleation rate agrees with the theoretical value obtained by the classical theory using reduced surface tension. In the present calculations, $\sigma_*=0.7\sigma$ is assumed [30,31]. In the present calculations, $r_c=1.0\times10^{-9}$(m) is assumed for simplicity though rigorously it depends on temperature and vapor pressure [29,30]. The change of the number of droplets inside the bubble (ΔN) in time Δt is calculated by Eq. (34):

$$\Delta N=\frac{4}{3}\pi R^3 J\Delta t+\left(\frac{3\dot m N}{\rho_L R}\Delta t\right)-\left(\frac{4\pi r_*^2\dot m}{\frac{4}{3}\pi r_*^3\rho_L}\Delta t\right), \tag{34}$$

where N is the total number of droplets inside the bubble. The first term of right-hand side of Eq. (34) is the nucleation of droplets by condensation of nitrogen vapor inside the bubble. The second term is the reduction due to the deposit of the droplets onto the bubble wall [30]. The second term is included only when $N>0$ and $\dot m<0$, otherwise it is replaced by zero. The third term is the reduction of droplets by evaporation. The third term is included only when $N>0$ and $\dot m>0$, otherwise it is replaced by zero. In the present model, the radius of a droplet is assumed to be a constant [$r_*=r_c=1.0\times10^{-9}$ m] for simplicity. For rigorous discussions, the change of the size of a droplet due to evaporation or condensation should be taken into account [29,30]. $\Delta' N$ in Eqs. (6) and (19) is expressed by the first and the third terms of the right-hand side of Eq. (34):

$$\Delta' N=\frac{4}{3}\pi R^3 J\Delta t-\left(\frac{4\pi r_*^2\dot m}{\frac{4}{3}\pi r_*^3\rho_L}\Delta t\right). \tag{35}$$

The total volume of droplets (V_d) in Eq. (2) is calculated simply by

$$V_d=\tfrac{4}{3}\pi r_*^3 N. \tag{36}$$

Following is the calculation method of bubble shape oscillations. In the present study, the formulation of Brenner *et al.* [32,33] is employed. A distortion of the spherical interface is expressed by $R(t)+a_n(t)Y_n$, where Y_n is a spherical harmonic of degree n and $a_n(t)$ is the distortion amplitude. The dynamics of $a_n(t)$ is given by [32,33]

$$\ddot a_n+B_n(t)\dot a_n-A_n(t)a_n=0, \tag{37}$$

where

$$A_n(t)=(n-1)\frac{\ddot R}{R}-\frac{\beta_n\sigma}{\rho_L R^3}-\left[(n-1)(n+2)+2n(n+2)(n-1)\frac{\delta}{R}\right]\frac{2\mu\dot R}{R^3} \tag{38}$$

and

$$B_n(t)=3\frac{\dot R}{R}+\left[(n+2)(2n+1)-2n(n+2)^2\frac{\delta}{R}\right]\frac{2\mu}{R^2}, \tag{39}$$

where $\beta_n=(n-1)(n+1)(n+2)$, and δ is the thickness of the thin layer around the bubble where fluid flows [32,33]:

$$\delta=\min\left(\sqrt{\frac{\mu}{\omega}},\frac{R}{2n}\right). \tag{40}$$

In order to take into account microscopic fluctuations, a random displacement of size 0.1 nm is added to the distortion $a_n(t)$ after each integration time step [33].

III. RESULTS

In the experiments of Baghdassarian, Cho, Varoquaux, and Williams [17], the amplitude of the acoustic wave was

TABLE I. Physical quantities of liquid nitrogen used in the calculations. μ is the viscosity, σ is the surface tension, c is the sound speed, ρ_L is the density, κ_L is the thermal conductivity, L is the latent heat of vaporization, and c_p is the specific heat at constant pressure.

μ (m^2/s)	2.33×10^{-7}
σ (N/m)	1.0×10^{-2}
c (m/s)	9.84×10^{2}
ρ_L (kg/m^3)	8.57×10^{2}
κ_L (W/m K)	1.4×10^{-1}
L (J/kg)	2.0×10^{5}
c_p (J/kg K)	2.0×10^{3}

varied from the lowest one to the highest one in the range for trapping a bubble at the pressure antinode of the standing wave in a cylindrical flask filled with liquid nitrogen. Only relative values of the acoustic amplitude are given and the absolute values are not given in Ref. [17]. The frequency of the acoustic wave is 28.5 kHz [17]. The ambient liquid temperature and pressure are $T_\infty = 66.5$ K and $p_\infty = 1.2$ bar, respectively [17]. The physical quantities of liquid nitrogen used in the present calculations are listed in Table I. Firstly, we will see a case of the higher acoustic drive, though the anomalous behavior of the light scattering from the bubble was observed in the lower drive cases [17].

A. Higher acoustic drive

When the amplitude (A) of the acoustic wave (ultrasound) is above 1.0 bar, the computer simulations show that a bubble of any size suffers the shape instability and that it seems to be destroyed when the criterion is given by [33]

$$\max\left(\frac{|a_n|}{R}\right) \geqslant 1, \tag{41}$$

where a_n is the distortion amplitude of the spherical harmonic of degree n. The highest amplitude of the acoustic wave for spherical oscillations is 1.0 bar and the largest equilibrium bubble radius (R_0) is 3 μm under the condition. The calculated results for $A = 1.0$ bar and $R_0 = 3$ μm are shown in Figs. 1(b)–1(h) as functions of time for one acoustic cycle (35.1 μs). The time axes are the same throughout Figs. 1(a)–1(h). In Fig. 1(a), the pressure of the acoustic wave [$p_s(t)$] is shown. In Fig. 1(b), the bubble radius (R) is shown; the line is the calculated result and the dash-dotted line is the experimental data [17]. It should be noted that the experimental data in Ref. [17] are normalized to the maximum radius and in Fig. 1(b) they are converted to the real values by the scale $1 \rightarrow 9.5$ μm. It is seen that the calculated result and the experimental data fit well especially at the collapse phase of the bubble oscillation. The bounces after the strongest collapse are much smaller than those observed for a SBSL bubble in water [24,28]. It is due to the small size (3 μm) of the bubble which results in the stronger damping of oscillations by thermal conduction [34].

In Fig. 1(c), the temperature inside the bubble (T) is shown. It is seen that the bubble oscillation is nearly the isothermal process and that the maximum temperature rise is only 5 K, which is much lower than that required for sonoluminescence [6,9,15]. In Fig. 1(d), the liquid temperature at bubble wall ($T_{L,i}$) is shown with the same vertical axis as that of Fig. 1(c). It is seen that $T_{L,i}$ is also almost constant and that the maximum temperature rise is less than 5 K. The low temperature rise of T and $T_{L,i}$ at the collapse is due to the low speed of the collapse ($|\dot{R}|$) shown in Fig. 1(e) compared with the recently measured value (350 m/s) of a SBSL bubble in water [35]. It is due to the higher saturated vapor pressure of liquid nitrogen at 66.5 K ($p_v^* = 2.3\times10^4$ Pa) compared with that of water at room temperature ($p_v^* = 2.3\times10^3$ Pa). The pressure inside the bubble (p_g) is always larger than the saturated vapor pressure (p_v^*) and the collapse is made milder by the higher pressure inside the bubble in liquid nitrogen. It should be noted that even at the freezing point of liquid nitrogen (63 K) the saturated vapor pressure (1.3×10^4 Pa) is much larger than that of water at room temperature (2.3×10^3 Pa). Thus it seems difficult to observe a SBSL in liquid nitrogen.

In Fig. 1(f), the number of molecules inside the bubble is shown with the logarithmic vertical axis. It is seen that strong evaporation of nitrogen takes place at the expansion of the bubble in order to maintain the vapor pressure to the saturated one. On the contrary, strong condensation takes place at the bubble collapse in order also to maintain the vapor pressure to the saturated one [36]. The number of helium molecules inside the bubble is assumed to be constant in the present study because the diffusion of gas is a very slow process compared with the bubble oscillations [18,34].

In Fig. 1(g), the pressure inside the bubble (p_g) is shown with the logarithmic vertical axis. It is seen that the pressure rise at the collapse is much smaller than that of a SBSL bubble in water [18,36], which is again due to the milder collapse. In Fig. 1(h), the vapor pressure (p_v) inside the bubble is shown with the same vertical axis as that of Fig. 1(g). It is seen that p_v is maintained nearly to the saturated value at 66.5 K ($p_v^* = 2.3\times10^4$ Pa). At the collapse, p_v increases a little due both to the nonequilibrium effect of condensation and to the increase of the liquid temperature, which results in the higher saturated vapor pressure (p_v^*).

The number of droplets created inside the bubble is less than 2 in this case and the effect of the droplets formation is negligible on bubble dynamics.

B. Lower acoustic drive

For lower amplitude of the acoustic wave, the anomalous behavior of the intensity of the scattered light is observed in the experiment [17], which is shown in Fig. 2(b) by the dash-dotted line. Baghdassarian, Cho, Varoquaux, and Williams [17] converted the observed intensity of the scattered laser beam from the bubble to the bubble radius by Mie theory of scattering that the scattered intensity is proportional to R^2. The experimental data in Ref. [17] is normalized to the maximum ''radius'' and in Fig. 2(b) the data are converted to real values by the scale $1 \rightarrow 25.0$ μm. In Figs. 2(b)–2(e), the calculated results for $A = 0.7$ bar and $R_0 = 10$ μm are shown as functions of time for one acoustic cycle (35.1 μs). When $R_0 > 10$ μm, a bubble suffers the shape instability.

In Fig. 2(a), the pressure of the acoustic wave [$p_s(t)$] is shown. The time axes are the same throughout Figs. 2(a)–

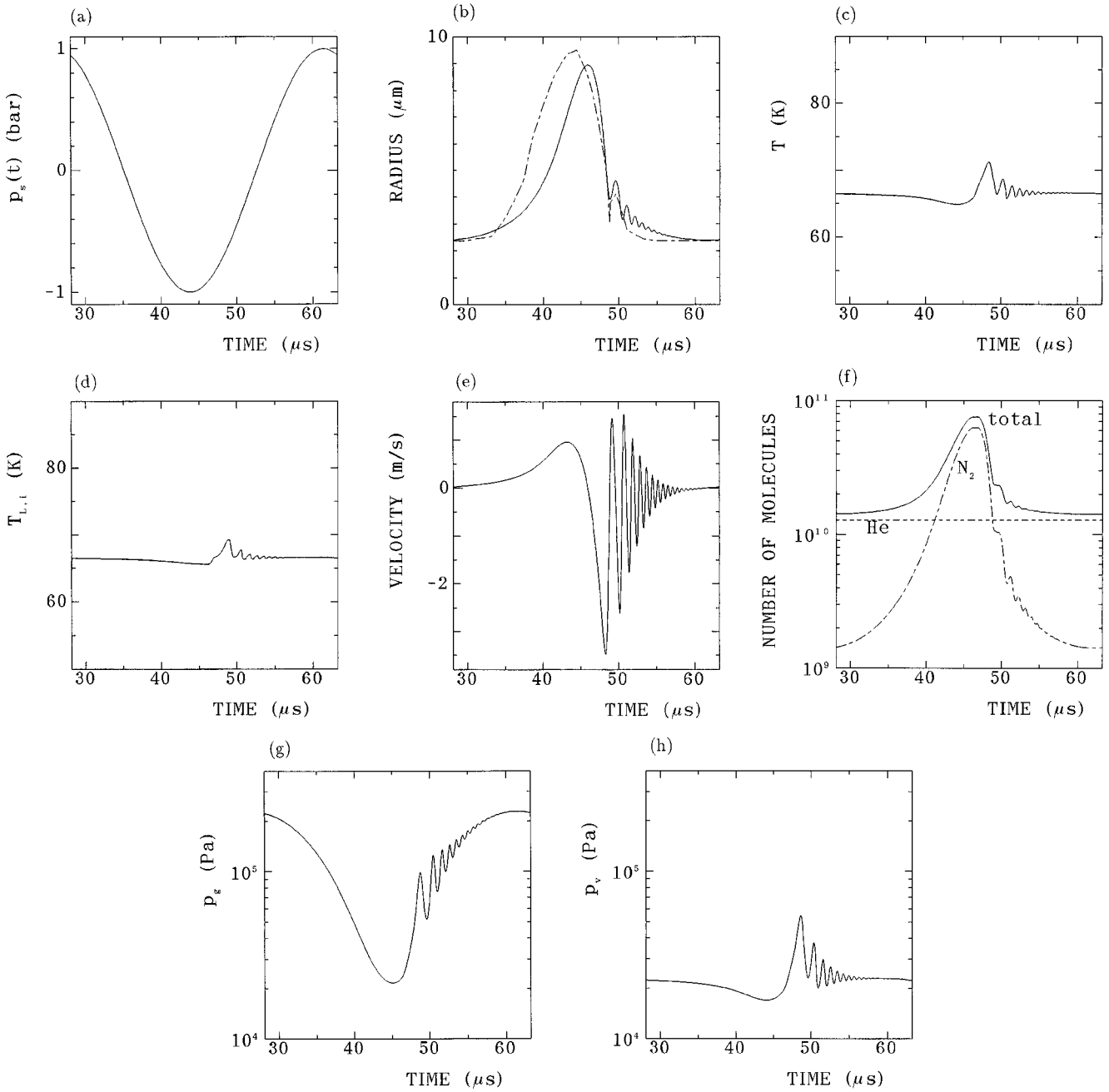

FIG. 1. Calculated results for one acoustic cycle for a case of the higher acoustic drive ($A=1.0$ bar). The equilibrium bubble radius is 3 μm. The time axes are the same throughout the figures. (a) The pressure of the acoustic wave [$p_s(t)$]. (b) The bubble radius (R). The line is the calculated result and the dash-dotted line is the experimental data [17]. (c) The temperature inside the bubble (T). (d) The liquid temperature at the bubble wall ($T_{L,i}$) with the same vertical axis as that of (c). (e) The bubble wall velocity ($\dot{R}$). (f) The number of molecules inside the bubble with logarithmic vertical axis. The solid line is the total number of molecules (n_t), the dash-dotted line is the number of vapor molecules (n_{N_2}), and the dotted line is that of helium molecules (n_{He}). (g) The pressure inside the bubble (p_g) with the logarithmic vertical axis. (h) The vapor pressure inside the bubble (p_v) with the same vertical axis as that of (g).

2(e). From Fig. 2(b), it is seen that the calculated result of the radius-time curve(line) and the experimental data(dash-dotted line) differ even qualitatively. The behavior of the experimentally obtained ''radius''-time curve is very strange because it changes wildly and it takes large values when the pressure of the acoustic wave [Fig. 2(a)] is large though it usually results in smaller radius. This mystery is solved by Fig. 2(c). It is seen that an appreciable amount of fine droplets are created inside the bubble when the radius [line in Fig. 2(b)] is small. In reality, the number of fine droplets created inside the bubble is much larger than that estimated in the present calculation because the nucleation rate of smaller droplets is much larger than that of droplets of 1 nm in radius assumed in the present calculation, according to Eq. (33). The Rayleigh scattering by a single fine droplet of 1 nm radius or less is negligible compared to the light scattering by a bubble of 10 μm radius [37,38]. However, the concentration fluctuations of such many fine droplets in regions comparable to the wavelength of the light (0.5 μm) in size cause much stronger light scattering than that by a single fine

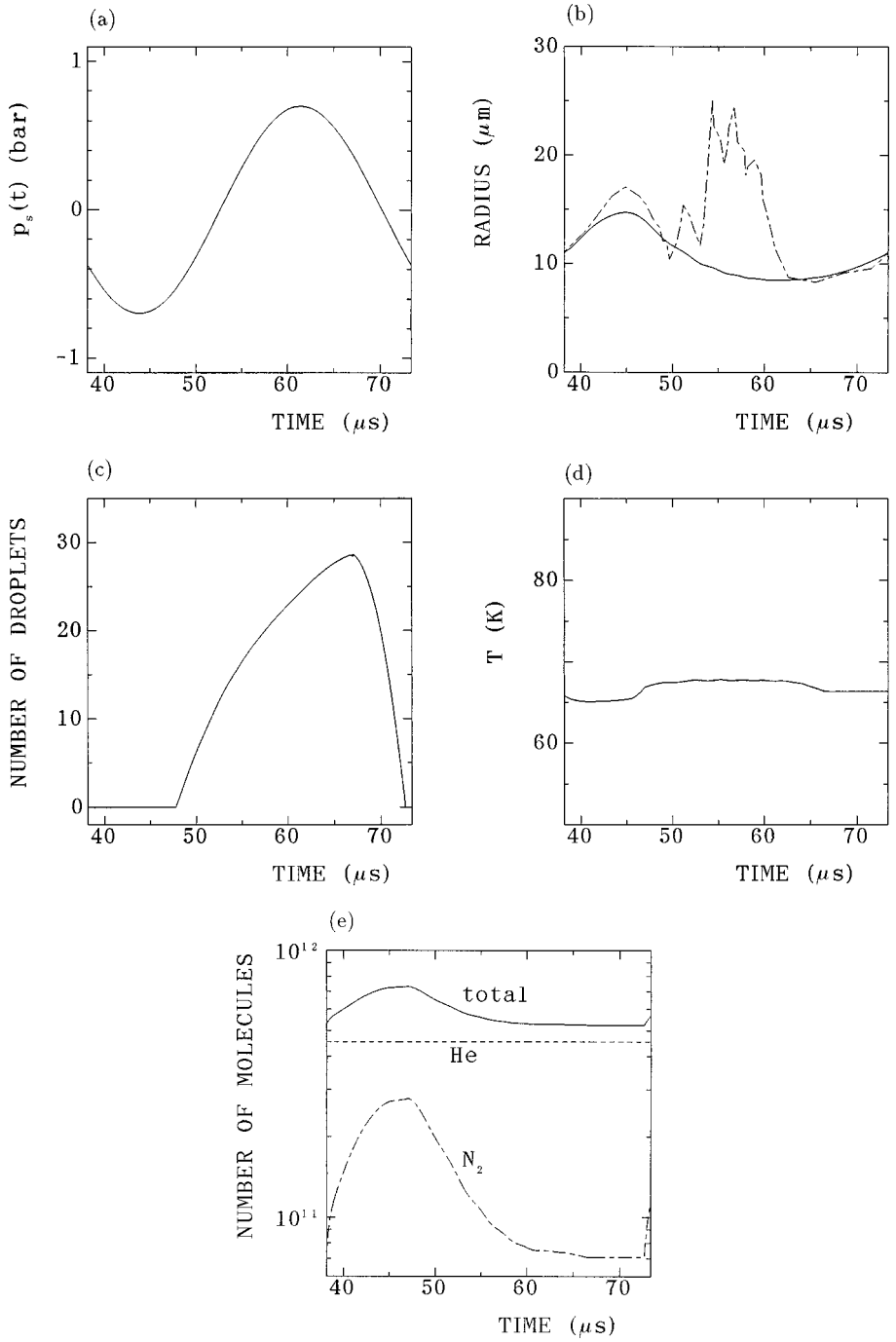

FIG. 2. Calculated results for one acoustic cycle for a case of the lower acoustic drive ($A=0.7$ bar). The equilibrium bubble radius is 10 μm. The time axes are the same throughout the figures. (a) The pressure of the acoustic wave [$p_s(t)$]. (b) The bubble radius (R). The line is the calculated result and the dash-dotted line is the experimental data [17]. (c) The number of droplets inside the bubble (N). (d) The temperature inside the bubble (T) with the same vertical axis as those of Figs. 1(c) and 1(d). (e) The number of molecules inside the bubble with logarithmic vertical axis. The solid line is the total number of molecules (n_t), the dash-dotted line is the number of vapor molecules (n_{N_2}), and the dotted line is that of helium molecules (n_{He}).

droplet [37,38]. Thus it is suggested that the anomalous behavior of the intensity of the scattered light [dash-dotted line in Fig. 2(b)] is due to the scattering by fine droplets inside the bubble. In order to discuss more quantitatively the scattering by droplets, improved numerical simulations of droplets formation and reduction are required, including the effect of growth or shrinkage of droplets by condensation or evaporation using the rigorous critical radius (r_c) given in Refs. [29, 30]. By such the simulations, peaks seen in the experimental data [dash-dotted line in Fig. 2(b)] may be explained. However, it should be noted that the shape oscillations of a bubble might alternatively cause the anomalous light scattering.

In Fig. 2(d), the temperature inside the bubble is shown with the same vertical axis as those of Figs. 1(c) and 1(d). It is seen that the bubble oscillation in this case is also a nearly isothermal process. In Fig. 2(e), the number of molecules inside the bubble is shown with the logarithmic vertical axis.

TABLE II. The coefficients for Eq. (A1).

$N_1 = -5.07$
$N_2 = 13.68$
$N_4 = -11.94$
$N_6 = 2.64$
$N_{10} = -0.378$
$N_{13} = 0.076$

It is seen that evaporation takes place at the expansion of the bubble and that condensation takes place at the collapse as in the case of the higher acoustic drive. The effect of droplet formation and evaporation is negligible on the change of the number of nitrogen molecules because the total number of nitrogen molecules forming the droplets is less than 10^4.

IV. CONCLUSION

Computer simulations of bubble oscillations in liquid nitrogen are performed for a single helium bubble, including the effect of evaporation and condensation of nitrogen vapor at the bubble wall, that of droplets formation inside the bubble, and that of the thermal conduction both inside and outside the bubble. It is clarified that in the case of the lower acoustic drive ($A = 0.7$ bar) an appreciable amount of fine droplets are created inside the bubble, which may result in the enhancement of the scattering of laser beam monitoring the bubble oscillations in the experiment of Baghdassarian, Cho, Varoquaux, and Williams [17]. It is also clarified that the speed of the bubble collapse in liquid nitrogen under a condition of stable oscillations is much less than that of a SBSL bubble in water. The milder collapse in liquid nitrogen is due to the larger saturated vapor pressure and it results in much lower maximum temperature attained in the bubble than that required for SBSL.

ACKNOWLEDGMENTS

The author thanks Professor G. A. Williams for sending the experimental data of radius-time curves of a bubble in cryogenic fluids.

APPENDIX: THE SATURATED VAPOR PRESSURE OF LIQUID NITROGEN

The saturated vapor pressure (p_v^*) of liquid nitrogen is calculated as a function of temperature by the empirical formula given in Ref. [39]:

$$p_v^*/P_c = (T/T_c)(1 + N_1\tau + N_2\tau^{1.9} + N_4\tau^{2.4} + N_6\tau^{3.5} + N_{10}\tau^{5.5} + N_{13}\tau^7) \quad \text{(A1)}$$

where $\tau = [(T_c/T) - 1]$, and P_c and T_c are the critical pressure and temperature, respectively. The values of P_c and T_c used for this equation are 3.3978 MPa and 126.193 K, respectively. The coefficients (N_i) are listed in Table II.

[1] D. F. Gaitan, L. A. Crum, C. C. Church, and R. A. Roy, J. Acoust. Soc. Am. **91**, 3166 (1992).
[2] B. P. Barber and S. J. Putterman, Nature (London) **352**, 318 (1991).
[3] L. A. Crum, Phys. Today **47** (9), 22 (1994).
[4] B. P. Barber, R. Hiller, K. Arisaka, H. Fetterman, and S. Putterman, J. Acoust. Soc. Am. **91**, 3061 (1992).
[5] B. Gompf, R. Günther, G. Nick, R. Pecha, and W. Eisenmenger, Phys. Rev. Lett. **79**, 1405 (1997).
[6] R. Hiller, S. J. Putterman, and B. P. Barber, Phys. Rev. Lett. **69**, 1182 (1992).
[7] R. Hiller, Ph.D. thesis, University of California, 1995.
[8] D. F. Gaitan *et al.*, Phys. Rev. E **54**, 525 (1996).
[9] C. C. Wu and P. H. Roberts, Phys. Rev. Lett. **70**, 3424 (1993).
[10] L. A. Crum, J. Acoust. Soc. Am. **95**, 559 (1994).
[11] W. C. Moss, D. B. Clarke, J. W. White, and D. A. Young, Phys. Fluids **6**, 2979 (1994).
[12] L. Kondić, J. I. Gersten, and C. Yuan, Phys. Rev. E **52**, 4976 (1995).
[13] V. Q. Vuong and A. J. Szeri, Phys. Fluids **8**, 2354 (1996).
[14] H. Kwak and J. H. Na, Phys. Rev. Lett. **77**, 4454 (1996).
[15] K. Yasui, Phys. Rev. E **56**, 6750 (1997).
[16] M. Bernard, M. Fauver, and G. A. Williams, Physica B **194–196**, 165 (1994).
[17] O. Baghdassarian, H. Cho, E. Varoquaux, and G. A. Williams, J. Low Temp. Phys. **110**, 305 (1998).
[18] K. Yasui, J. Acoust. Soc. Am. **98**, 2772 (1995).
[19] P. W. Atkins, *Physical Chemistry*, 2nd ed. (Oxford University Press, New York, 1982).
[20] M. N. Kogan, *Rarefied Gas Dynamics* (Plenum, New York, 1969).
[21] Y. S. Touloukian, P. E. Liley, and S. C. Saxena, *Thermal Conductivity* (IFI/Plenum, New York, 1970).
[22] R. W. Schrage, *A Theoretical Study of Interphase Mass Transfer* (Columbia University Press, New York, 1953).
[23] S. Fujikawa and T. Akamatsu, J. Fluid Mech. **97**, 481 (1980).
[24] K. Yasui, J. Phys. Soc. Jpn. **65**, 2830 (1996).
[25] J. O. Hirschfelder, C. F. Curtiss, and R. B. Bird, *Molecular Theory of Gases and Liquids* (John Wiley & Sons, New York, 1954).
[26] Y. S. Touloukian and T. Makita, *Specific Heat* (IFI/Plenum, New York, 1970).
[27] K. Yasui, J. Phys. Soc. Jpn. **66**, 2911 (1997).
[28] B. P. Barber and S. J. Putterman, Phys. Rev. Lett. **69**, 3839 (1992).
[29] J. Frenkel, *Kinetic Theory of Liquids* (Dover, New York, 1955).
[30] Y. Matsumoto and A. E. Beylich, Trans. ASME J. Fluids Eng. **107**, 281 (1985).
[31] H. Kawada and Y. Mori, Bull. JSME **16**, 1053 (1973).
[32] M. P. Brenner, D. Lohse, and T. F. Dupont, Phys. Rev. Lett. **75**, 954 (1995).

[33] S. Hilgenfeldt, D. Lohse, and M. P. Brenner, Phys. Fluids **8**, 2808 (1996).
[34] T. G. Leighton, *The Acoustic Bubble* (Academic, London, 1994).
[35] G. A. Dalgadino and F. J. Bonetto, Phys. Rev. E **56**, R6248 (1997).
[36] K. Yasui (unpublished).
[37] H. C. van de Hulst, *Light Scattering by Small Particles* (Dover, New York, 1981).
[38] M. J. Vold and R. D. Vold, *Colloid Chemistry* (Reinhold, New York, 1964).
[39] R. T. Jacobsen, R. B. Stewart, and M. Jahangiri, J. Phys. Chem. Ref. Data **15**, 735 (1986).